A Model Predictive Power Control Method for PV and Energy Storage Systems with Voltage Support Capability

Shan, Yinghao; Hu, Jiefeng; Guerrero, J. M.

Published in:
IEEE Transactions on Smart Grid

DOI (link to publication from Publisher):
10.1109/TSG.2019.2929751

Publication date:
2020

Document Version
Accepted author manuscript, peer reviewed version

A Model Predictive Power Control Method for PV and Energy Storage Systems with Voltage Support Capability

[1]Yinghao Shan, *Student Member, IEEE,* Jiefeng Hu, *Senior Member, IEEE,* and Josep M. Guerrero, *Fellow, IEEE*

***Abstract*—The cascaded control method with an outer voltage loop and an inner current loop has been traditionally employed for the voltage and power control of photovoltaic (PV) inverters. This method, however, has very limited power regulation capability. With the fast increasing penetration of PV power generation systems in the distribution network, the voltage rise/drop has become a serious problem impacting negatively on the power quality and grid stability. Therefore, flexible power regulation is highly desired for PV inverters to provide ancillary services. This paper proposes a novel model predictive power control (MPPC) scheme to control and coordinate the dc-dc converter and inverter for grid-connected PV systems with energy storage systems (ESS). By regulating the dc-bus voltage and controlling the active and reactive power flows, MPPC can support the power grid to maintain stable voltage and frequency and improve the power factor. Numerical simulation and controller hardware-in-the-loop (CHIL) testing have been conducted on a PV-ESS system to verify the capability and effectiveness of the proposed control strategy.**

***Index Terms*—Model predictive control, dc-dc bidirectional converter, dc-ac converter, voltage support.**

I. Introduction

For environment protection by reducing the greenhouse gas emissions, numerous government policies have been established to encourage the use of renewable energy sources. As one of the most promising renewable energy sources, the global solar photovoltaic (PV) power capacity has been increasing rapidly. According to the International Energy Agency (IEA), by 2050, the solar PV power generation will contribute 16% of the world's electricity, and 20% of that capacity will come from residential installations [1].

Because of the intermittent power generation, PV systems must be equipped with energy storage systems (ESS) to achieve smooth power flows [2], and connected to the power grid for reliable power supply. In grid integration, the power electronic converter plays an important role to interface between the power grid and renewable energy sources [3], [4]. Fig.1 shows a typical PV-ESS configuration. The boost converter is used to achieve maximum power point tacking (MPPT) for the PV panels. The bidirectional dc-dc converter is controlled to absorb excess energy by charging or supply additional energy by discharging the ESS. The grid-connected inverter converts the dc-bus voltage into the ac grid voltage.

For PV system control, the cascaded linear control method has been widely used for decades [5]. This control structure requires multiple feedback loops and PWM modulation, resulting in relatively slow dynamic response. In a practical PV power plant, the fluctuating PV panel output can cause oscillations in the dc-bus voltage, and deteriorate the power quality on the ac side. As a result, the traditional cascaded control is ineffective to deal with this fluctuation. Another concern is the power flow between the PV system and utility grid, which is usually handled by the grid-connected inverters. Traditionally, the cascaded feedback loops with PID controllers are adopted to control the ESS dc-dc converter and the grid-connected inverter [6]-[11]. To regulate the ESS charging or discharging current, an inner current control loop is commonly employed [6]-[8]. For the grid-connected inverter, an outer voltage loop is used to maintain the dc-bus voltage with the *d*-axis current reference as the output. In the inner current loop, the *d*-axis current is controlled to regulate the active power flow, and the *q*-axis current to regulate the reactive power flow [9]-[11]. Usually, the *q*-axis current reference is set to zero for unity power factor operation. In this conventional control strategy, the flexible power regulation capability is limited because both the active and reactive power flows between the PV system and the grid cannot be controlled directly. With the fast increasing penetration of PV systems in the distribution network, the voltage rise/drop has become a problem which impacts negatively on the power quality and grid stability [12], [13]. Therefore, flexible power regulation is highly desired for PV inverters to provide ancillary services.

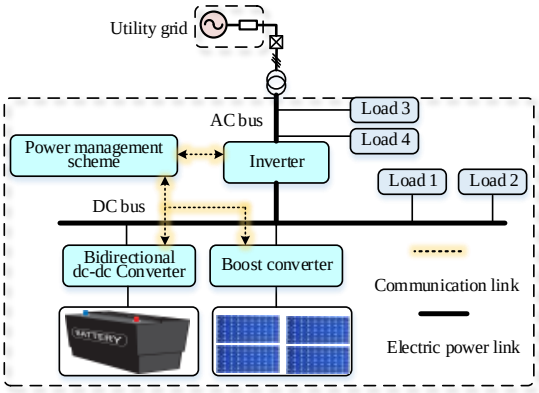

Fig.1. A PV-ESS configuration.

To achieve flexible power regulation, the PV system control method must be modified to control the active and reactive power flows injected in the point of common coupling (PCC) with the grid. In the past few years, the model predictive control (MPC) scheme, in which the optimal switching state of power converter

[1] [1]This work is supported in part by Hong Kong Research Grants Council under Grants PolyU252040/17E and PolyU152064/19E, and in part by The Hong Kong Polytechnic University under Grants 1-ZE7J and G-YBZ4. (Corresponding Author: Jiefeng Hu)

Y. Shan and J. Hu are with the Department of Electrical Engineering, The Hong Kong Polytechnic University, Hung Hom, Hong Kong (e-mail: jerry.hu@polyu.edu.hk).

J. M. Guerrero is with the Department of Energy Technology, Aalborg University, Aalborg DK-9220, Denmark (e-mail: joz@et.aau.dk)

is determined according to a specified cost function, has been adopted to obtain better converter performance than PID control [14]-[17]. Although some system level algorithms have been proposed to achieve a variety of goals such as minimal system operating costs [18], optimal power flow management [19], economic load dispatch [20], realizing voltage coordination [21], and stabilizing terminal voltages [22], the MPC is seldom reported in the coordinated control of multiple converters in microgrids, and flexible power regulation for voltage support has not been studied. At the device level, a review of various MPC-controlled power converters is presented in [23,24]. However, as aforementioned, neither flexible power regulation nor voltage support is reported. In [25], a direct power control strategy using the MPC scheme is developed for grid-connected inverters in PV applications. Although flexible power regulation has been achieved, the intermittent nature of solar PVs and the energy storage are not considered. Besides, the relationship between power flow and voltage deviation is not investigated. Recently, an MPC method is proposed to smooth the PV output and stabilize the PCC voltage by controlling the ESS dc-ac converter [26]. However, only the active power of ESS is controlled while the reactive capacity of the PV inverter is unexplored. In [27], a double-loop control with an MPC-controlled inner loop and a PI-controlled outer loop is proposed for a dc-dc boost converter. However, the control loops are not fully MPC based, and not competent for ESS charging and discharging. In [28], an MPC approach is incorporated with the droop control method to control the parallel inverters in ac microgrids. Once again, the intermittent nature of renewable energy resources is not considered, and the grid-connected operation not studied. In [29], although the whole microgrid control is MPC based, the microgrid is working under islanded mode and the power regulation of the inverter is not investigated. So far, there is still a lack of device level research detailing the converter control techniques to achieve flexible power regulation for grid-connected PV systems.

In this paper, a new model predictive power control (MPPC) strategy is proposed to control and coordinate the bidirectional dc-dc converter and inverter in PV-ESS systems as shown in Fig.1. The active power is chosen as the control objective for the bidirectional dc-dc converter and both the active and reactive power flows as the control objectives of the grid-connected inverter. The MPPC method in ESS can smooth the PV fluctuating output and maintain the stability of dc-link voltage, and the MPPC scheme for the inverter can control flexibly the power flow between the PV-ESS system and the utility grid, such that the PV-ESS system can support the grid by compensating the voltage to a certain degree.

Currently, there are several reports devoted to the MPC-based system-level stability [21,30,31]. However, to date, to the authors' best knowledge, it is still an open question about the robustness and stability analysis of device-level MPC control of power converters [23,24]. Carrying out extensive simulations under different key control parameters is an effective way to evaluate the robustness and stability of the designed MPC controllers [23,28]. In this study, the robustness and stability are estimated by gradually varing filter settings. It is proved that the proposed MPPC scheme is highly stable and robust, as well as invulnerable to parameter variations. After that, the system performance are also examined with a longer-horizon prediction and compared with existing MPC methods. The results show that the proposed MPPC scheme is indeed feasible and effective using only one-step prediction. In addition, the proposed MPPC scheme is superior to existing MPC combinations in terms of maintaining a stable dc-bus voltage and providing a flexible power regulation.

Our major contributions in the study are outlined as follows.

1) The bidirectional dc-dc converter and the inverter in PV-ESS systems can be controlled and coordinated with the proposed MPPC scheme under grid-connected operation to achieve a flexible power regulation. The possibility of maintaining the dc-bus voltage by controlling the bidirectional dc-dc converter rather than the inverter is studied so that the control freedom of the inverter on the active and reactive powers, to some extent, can be fully explored.

2) The voltage support via regulating power flow is also investigated with quantized power correction values. Thus, the voltage dips are compensated to provide a high-quality power supply, which substantially extends the potential and capability of device-level converters.

The remainder of this paper is organized as follows. Section II describes the proposed MPPC scheme. Section III presents the power flow control for voltage support. In Section IV, the proposed MPPC scheme is numerically simulated and the comparison is made. The experimental tests are provided in Section V. Finally, Section VI concludes the paper.

II. Proposed Model Predictive Power Control (MPPC)

A. Control of Bidirectional Buck-boost Converters

Traditionally, in a grid-connected PV system, the dc-bus voltage is maintained by using an inverter, and a buck-boost converter is used to regulate the ESS charging/discharging current to smooth the PV output. This control structure limits the flexible power regulation capability of PV-ESS system because the active and reactive power flows between the PV-ESS system and the grid cannot be controlled directly and flexibly. The question has now become whether it is possible to maintain the dc-bus voltage by controlling the dc-dc buck-boost converter rather than the inverter so that the control freedom of the inverter on the bidirectional active and reactive power flows can be fully explored?

To provide a positive answer to the above question, an in-depth analysis of the system model is performed. Fig.2 shows the ESS schematic configuration, where a dc-dc converter is used to interface the low voltage (LV) bus, which is connected to the battery, and the high voltage (HV) bus, also known as the dc-link. Fig.3 shows the equivalent circuits of (a) boost and (b) buck modes, respectively. If S_2 is switching (1 or 0) as a main process and S_1 is complementary, it operates in the boost mode (Fig.3(a)). The battery supplies power to the dc-link through discharging. On the contrary, if S_1 is switching (1 or 0) as a main process and S_2 is complementary, it operates in the buck mode (Fig.3(b)). The battery is charged with absorbing power from the dc-link.

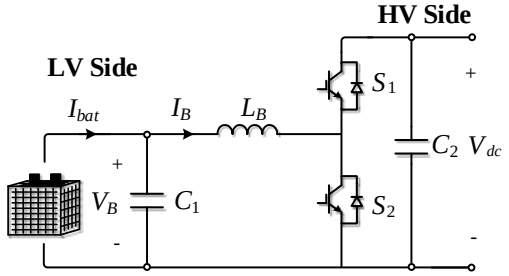

Fig.2. Schematic diagram of the ESS.

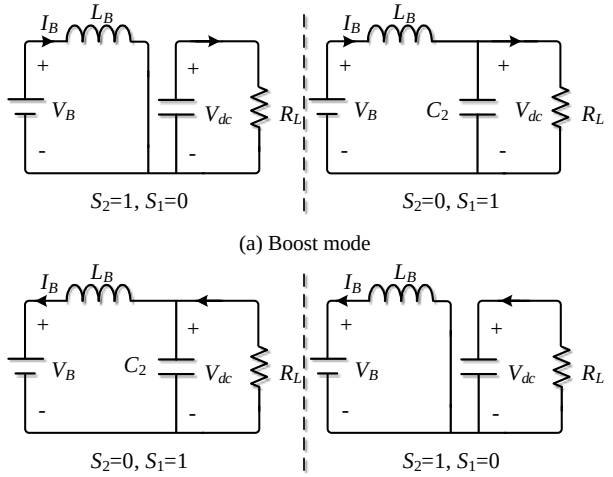

Fig.3. Equivalent circuits of (a) boost and (b) buck modes.

In the boost operation, the circuit model is expressed as

$$\begin{cases} S_2=1, S_1=0: \ L_B\dfrac{dI_B}{dt}=V_B \\ S_2=0, S_1=1: \ L_B\dfrac{dI_B}{dt}=V_B-V_{dc} \end{cases} \tag{1}$$

The discrete-time model for a sampling time T_s can be written as:

$$\begin{cases} S_2=1, S_1=0: \ I_B(k+1)=\dfrac{T_s}{L_B}V_B(k)+I_B(k) \\ S_2=0, S_1=1: \ I_B(k+1)=\dfrac{T_s}{L_B}(-V_{dc}(k)+V_B(k))+I_B(k) \end{cases} \tag{2}$$

Correspondingly, the discrete-time models of the buck operation can be described as:

$$\begin{cases} S_2=0, S_1=1: I_B(k+1)=\dfrac{T_s}{L_B}(V_{dc}(k)-V_B(k))+I_B(k) \\ S_2=1, S_1=0: I_B(k+1)=-\dfrac{T_s}{L_B}V_B(k)+I_B(k) \end{cases} \tag{3}$$

Since the battery charging and discharging processes depend fundamentally on the current, it is necessary to know the relationship of currents in the entire system. Fig.4 illustrates the currents flowing between the renewable energy sources (RES), which is PV in this case, ESS and the rest of the microgrid (ROM).

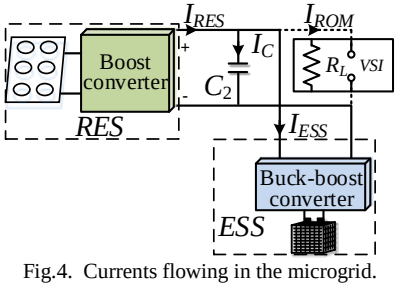

Fig.4. Currents flowing in the microgrid.

By the Kirchoff's current law (KCL), one obtains

$$I_{ESS}=I_{RES}-I_C-I_{ROM} \tag{4}$$

where I_{ESS} is the charging/discharging current of ESS (assuming charging as the positive direction), I_{ROM} the current flowing into the dc loads and the dc-ac voltage source inverter (VSI), I_{RES} the current from the renewable (PV) energy source, and I_C the dc-bus capacitor current. Therefore, the required power from ESS to keep the system power balance can be determined by

$$P_{ESS}^*=\left|I_{ESS}\cdot V_{dc}^*\right| \tag{5}$$

where V_{dc}^* is the dc-bus voltage reference. Conforming to the capacitor characteristic, the dc-bus capacitor current at the (k+1)th time step can be predicted by

$$I_C(k+1)=\frac{1}{N}\left(\frac{C_2}{T_s}(V_{dc}^*-V_{dc}(k))\right) \tag{6}$$

where N is an integer coefficient utilized to limit the capacitor current [15], C_2 the capacitance of dc-bus capacitor, and $V_{dc}(k)$ the dc-bus voltage at the kth time step. Substituting (6) into (4) and assuming that I_{RES} and I_{ROM} are unchanged during a short period T_s, I_{ESS} at the next sampling instant can be predicted as

$$I_{ESS}(k+1)=I_{RES}(k)-\frac{1}{N}\left(\frac{C_2}{T_s}(V_{dc}^*-V_{dc}(k))\right)-I_{ROM}(k) \tag{7}$$

With the predicted ESS current, the required power of ESS in the next control instant can be computed by (5) and (7) as

$$P_{ESS}^*(k+1)=\left|\left[I_{RES}(k)-\frac{1}{N}\left(\frac{C_2}{T_s}(V_{dc}^*-V_{dc}(k))\right)-I_{ROM}(k)\right]\cdot V_{dc}^*\right| \tag{8}$$

Since the change of battery voltage is relatively slow and the battery output current is equal to its inductor current, the battery output power can be predicted as

$$P_{bat}(k+1)=\left|I_B(k+1)\cdot V_B(k)\right| \tag{9}$$

To keep the power balance, the required power of ESS should be provided/absorbed by the battery. Therefore, the cost function of MPPC in ESS can be formulated as

$$\begin{aligned} &J_P=\left|P_{ESS}^*(k+1)-P_{bat}(k+1)\right| \\ &s.t.\ SOC_{min}\le SOC\le SOC_{max},\ I_{bat}\le\left|I_{bat\_rated}\right| \end{aligned} \tag{10}$$

where SOC is the state of charge defined as

$$SOC=1-\frac{1}{Q_0}\int_0^t I_{bat}(t)dt\ ,$$

where Q_0 is the total amount of charge stored in a battery in Ah, t the time in seconds, and $I_{bat}(t)$ the battery current in A. Now it can be seen that the measurement and prediction of the dc-bus voltage are actually reflected in (8), and the control of the actual dc-bus voltage to track the reference is implemented in (10).

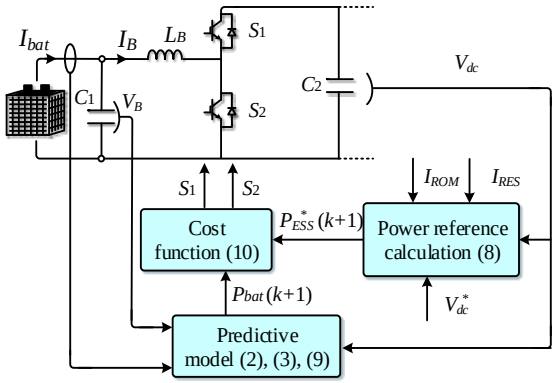

Fig.5. Block diagram of MPPC to control the dc-dc bidirectional converter

Fig.5 shows the proposed MPPC strategy for ESS. The required ESS power can be calculated jointly from the renewable energy source output current, I_{RES}, the dc load current and inverter input current, I_{ROM}, the actual dc-bus voltage, V_{dc}, and the reference dc-bus voltage, V_{dc}^*, by (8). Simultaneously, the battery voltage and

current and the actual dc-bus instant voltage will be used to predict the battery current $I_B(k+1)$, producing two possible values of $P_{bat}(k+1)$ by (2), (3) and (9). The optimal switching state that minimizes (10) will be chosen to control the buck-boost converter. Thus, the dc-bus voltage can be maintained stable as the common dc-link for PV-ESS and as the dc input for the dc-ac converter.

B. Control of Grid-Connected Inverters

Since the dc-bus voltage can be regulated by using the bidirectional buck-boost dc-dc converter of the ESS, the grid-connected inverter or the dc-ac converter can now be endowed with more control flexibility to provide ancillary services in the grid side. As to the dc-ac converter, depending on the switching ON/OFF states, it has eight voltage vectors for its outputs. Their complex forms can be described as

$$\boldsymbol{V}_i = \begin{cases} \frac{2}{3} V_{dc}^{*} e^{j(i-1)\frac{\pi}{3}} & (i = 1, 2, \cdots, 6) \\ 0 & (i = 0, 7) \end{cases} \tag{11}$$

Fig.6 presents the ac-side system. The mathematical model of dc-ac converter can be expressed in the space phasor form as

$$\boldsymbol{V}_i = \boldsymbol{V}_g + \boldsymbol{I}_f R_f + L_f \frac{d\boldsymbol{I}_f}{dt} \tag{12}$$

where $\boldsymbol{V}_i$ and $\boldsymbol{V}_g$ are the voltage vectors of the converter and the grid, respectively, $\boldsymbol{I}_f$ is the inductor current vector, R_f the equivalent resistance, and L_f the filter inductance.

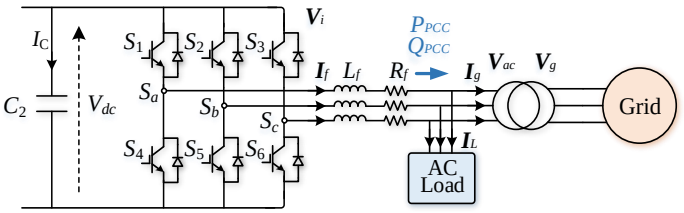

Fig.6. AC-side of microgrid

The output active and reactive power flows through the dc-ac converter into the ac common bus ($\boldsymbol{V}_{ac}$) or the PCC can be calculated by (in the $\alpha\beta$-plane)

$$P_{PCC} = \frac{3}{2}\mathrm{Re}\left\{\boldsymbol{V}_g \bar{\boldsymbol{I}}_f\right\} = \frac{3}{2}\left(V_{g\alpha} I_{f\alpha} + V_{g\beta} I_{f\beta}\right) \tag{13}$$

$$Q_{PCC} = \frac{3}{2}\mathrm{Im}\left\{\boldsymbol{V}_g \bar{\boldsymbol{I}}_f\right\} = \frac{3}{2}\left(V_{g\beta} I_{f\alpha} - V_{g\alpha} I_{f\beta}\right) \tag{14}$$

where $\bar{}$ represents the complex conjugate, Re{} the real component, and Im{} the imaginary component. The active and reactive power flows at the end of each sampling period can be predicted by (11) - (14) as [21]

$$P_{PCC}(k+1) = T_s\left[-\frac{R_f}{L_f}P_{PCC}(k) - \omega Q_{PCC}(k) + \frac{3}{2L_f}\left(\left|\boldsymbol{V}_g\right|^2 - \mathrm{Re}\left(\boldsymbol{V}_g \bar{\boldsymbol{V}}_i\right)\right)\right] + P_{PCC}(k) \tag{15}$$

$$Q_{PCC}(k+1) = T_s\left[\omega P_{PCC}(k) - \frac{R_f}{L_f}Q_{PCC}(k) - \frac{3}{2L_f}\mathrm{Im}\left(\boldsymbol{V}_g \bar{\boldsymbol{V}}_i\right)\right] + Q_{PCC}(k) \tag{16}$$

where ω is the grid frequency in radians. In the case of grid-tied mode, the active and reactive power flows are the control objectives, resulting in the following cost function to be minimized to assess the effects of each voltage vector on P_{PCC} and Q_{PCC} as

$$J_P = \left(P_{ref} - P_{PCC}(k+1)\right)^2 + \left(Q_{ref} - Q_{PCC}(k+1)\right)^2 \tag{17}$$

The proposed MPPC strategy for the dc-ac converter is presented in Fig.7. The grid voltage, $\boldsymbol{V}_g$, the inductor current vector, $\boldsymbol{I}_f$, and the converter voltage vectors, $\boldsymbol{V}_i$, are used to predict the next instant active and reactive powers. The selected switching states that can minimize (17) with the input active power reference P_{ref} and reactive power reference Q_{ref} are sent to the dc-ac converter to realize the control. A positive P_{ref} means that the active power flow from the grid to the dc-bus, and vice versa. The positive direction of the reactive power reference, Q_{ref}, is defined similarly. By specifying flexible P_{ref} and Q_{ref} in a certain range, the PV-ESS can support and compensate the grid voltage to some degree.

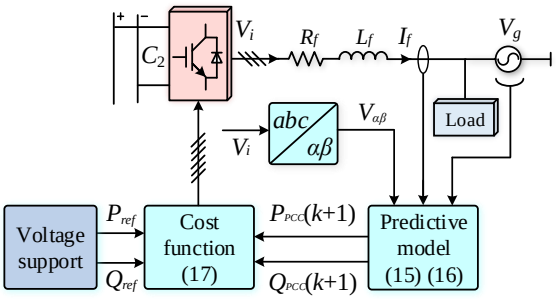

Fig.7. Block diagram of MPPC for the dc-ac converter connected to the grid.

III. Power Flow Control For Voltage Support

The proposed control strategy based on the MPPC algorithm provides a control freedom for the active and reactive powers. The remaining questions are how to take advantage of this flexible power regulation capability and how to set the active and reactive power references. In the traditional transmission and distribution system, the power flows are unidirectional from the upstream high voltage to downstream low voltage to supply the power load. In general, the transformer with an automatic voltage regulation tapping can realize the function of voltage regulation to deal with the voltage variation caused by the load change as well as the reverse power flow from the PV and ESS [32]. However, frequent operation of this kind of tapping will shorten the device lifetime and increase their maintenance requirements and costs. On the other hand, modifying the PV power system or operating it in a decentralized manner is often the simplest solution. Utilizing the PV inverter's flexible active and reactive power regulation capability is one of the emerging technologies to address the voltage regulation issue.

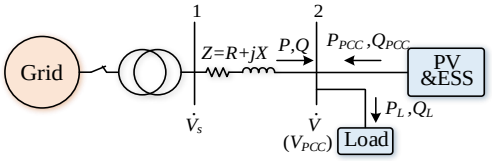

Fig.8. Single-line diagram of power flows.

Fig.8 shows a single-line radial distribution feeder, where Bus 1 is the bus of the distribution transformer located at the beginning of the feeder with voltage $\dot{V}_s$, Bus 2 the ac common bus (i.e. the PCC) of the microgrid with voltage $\dot{V}$, R and X are the feeder line resistance and reactance, the impedance $Z=R+jX$, and P and Q, P_{PCC} and Q_{PCC}, and P_L and Q_L are the active and reactive powers from the utility grid, the PV-ESS system, and the load, respectively, with the positive directions denoted in Fig.8. When Q_{PCC} is positive, the PV-ESS system releases the inductive reactive power, and when Q_{PCC} is negative, the PV-ESS system supplies the capacitive reactive power. Similary, when P_{PCC} is positive, the

PV-ESS system exports active power, and otherwise, the PV-ESS system imports active power.

According to the basic theory of power systems, the voltage drop from Bus 1 to Bus 2 can be expressed as

$$\Delta\dot{V} = \frac{RP + XQ}{\dot{V}} + j\frac{XP - RQ}{\dot{V}} \tag{18}$$

where the active and reactive powers satisfy

$$P = P_L - P_{PCC} \tag{19}$$

$$Q = Q_L - Q_{PCC} \tag{20}$$

Due to the high R/X ratio, the voltage drop equals approximately the real part of (18) as [33]

$$V = V_s - \frac{R(P_L - P_{PCC}) + X(Q_L - Q_{PCC})}{V} \tag{21}$$

Bus 2 voltage will change as the load changes. Especially, when there is a significant load change, the voltage will exceed the rated limit, endangering the safe operation of the grid. Thus, some measure should be taken to regulate the voltage. This study proposes a voltage support strategy by controlling both the active and reactive power flows. This method detects the real-time Bus 2 voltage. If there is a voltage drop caused by the load, it will send the deviation to the voltage support controller, and then the power correction signals (ΔP and ΔQ) are sent to the corresponding power references (P_{ref} and Q_{ref}). The power corrections can be calculated by

$$\Delta P = P_{ref} = (V_{t+1} - V_{t-1}) \times 100\% \times m_W \tag{22}$$

$$\Delta Q = Q_{ref} = (V_{t+1} - V_{t-1}) \times 100\% \times m_{Var} \tag{23}$$

where t+1 and t-1 mean one sampling time earlier and later than the instant when the load changes, and m_W and m_{Var} the coefficients of the active and reactive power flows, respectively. In such a way, the microgrid can provide active and reactive power compensation based on the PCC voltage variations. Equations (22) and (23) designed here are just simplified forms to test the potential grid support capability of the PV-ESS system. In the future smart grid framework with high PV penetration, the accurate amount of reactive power supplied by each microgrid should be determined by considering several factors including the grid voltage variations, transmission line R/X ratio, and the reactive capability of itself, etc.

The ΔP and ΔQ determined by (22) and (23) are then sent to the MPPC controller as the active and reactive power references, P_{ref}, Q_{ref}, as depicted in Fig.7. Due to the fast dynamic feature of the MPPC control algorithm, once the voltage deviation is detected, the corresponding active and reactive power flows can be injected into the grid to improve the voltage. Note that an inverter attached to a PV-ESS generator is not an infinite real power source or sink of reactive power, and the magnitudes of both active and reactive power flows are limited by the rated apparent power as shown by the phasor diagram in Fig.9.

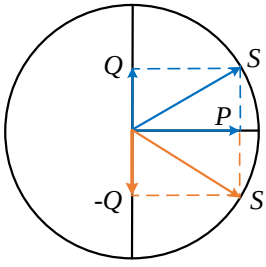

Fig.9. PV inverter capability model.

The range of allowable active power generation is given by

$$P \le P_{ESS\_\max} + P_{PV\_mpp} \tag{24}$$

where P_{ESS_max} is the power rating of the ESS, and P_{PV_mpp} the maximum PV power output. Once the actual active power is determined, the range of allowable reactive power generation can be obtained by

$$|Q| \le \sqrt{S^2 - P^2} \tag{25}$$

IV. Simulation

The PV-ESS system shown in Fig.1 is numerically simulated by using MATLAB/Simulink. Since the PV dc-dc converter and MPPT techniques have been widely studied, they are out of the scope of this work. In this paper, the effectiveness of the proposed MPPC scheme for grid-connected inverter and dc-dc bidirectional converter has been checked by simulation with the system parameters listed in Table I. Loads 1 and 2 are linear loads represented by using constant resistances, and Loads 3 and 4 the constant power type loads. The proposed MPPC scheme is compared with the traditional scheme of outer voltage and inner current loops of PI regulators. For a fair comparison, the converter average switching frequencies of the proposed method are the same as those of the traditional method. Since the sampling frequencies of both the proposed and conventional methods are 20kHz, the switching frequencies of the dc-dc and dc-ac converters are about 3.0kHz and 3.8kHz, respectively. For easy reference, the current flowing into the battery for charging is defined as the negative current in ESS, while the current flowing out of the battery for discharging is defined as the positive current. The active and reactive power flows between the PV-ESS system and the main grid are defined as P_{PCC} and Q_{PCC}, and the positive power flows are defined as from the main grid to the PV-ESS system.

A. Variable load demand

The capability of the proposed MPPC scheme coping with the variable load demand is verified for a scenario, in which P_{ref} and Q_{ref} are set as 0.8MW and 0MVar constant, and the solar irradiation and temperature at 600W/m^2 and 25℃, respectively, resulting in the total power output of about 1.5MW. Load 3 (0.5MW ac load) is connected to the ac-bus initially. Load 1 (0.5MW dc load) is switched on at 1s. Load 2 (1MW dc load) is switched on at 2s, and then switched off at 3s.

TABLE I System Parameters

Description	Value
Solar PV	SunPower Spr-305E-WHT-D, 2.5MW (STC)
ESS	Lithium-Ion battery, 300V, 2.3kAh, SOC_{max} = 90%, SOC_{min} = 10%, I_{bat_rated} = 3.5kA
DC-bus voltage	1.0kV
DC-bus capacitor	C_2 = 50mF
DC-side inductor	L_B = 0.17mH
AC-bus voltage	0.69kV (p-p), 60Hz
Transformer	25kV / 0.69kV (p-p), 60Hz
AC-bus LC filter	L_f = 0.6mH, R_f = 1.9mΩ
Linear loads	Critical load 1: 0.5MW, non-critical load 2: 1MW
Non-linear loads	Critical load 3: 0.5MW, non-critical load 4: 1MW
Voltage support	$m_W = -2.368\times10^5$, $m_{Var} = -1.259\times10^4$
PI gains of traditional method	
ESS	Current loop: k_p = 1.8, k_i = 1.1; Voltage loop: k_p = 12.3, k_i = 37.2 (f_{sw} = 3kHz)
Comparison MPC	k_p = 9, k_i = 122

Fig.10 shows the system performance of the proposed MPPC under variable load demand conditions, when the PV output is

fixed around 1.5MW by MPPT. The actual active and reactive power flows at PCC follow closely their references. While the load power is supplied by the main grid and PVs, the excess energy is absorbed by the ESS. When the load increases at 1s and 2s, the charging current of ESS decreases accordingly. The SOC keeps increasing as long as the load demand is smaller than the total power from the PVs and grid. The current passing through the PCC from the utility grid to the PV-ESS system is constant as the inverter is controlled with constant active and reactive power references. The dc-bus voltage is kept constant around its rated setpoint.

Fig.11 compares the dc-bus voltages controlled by the proposed method and the conventional method under the condition of same power generation and consumption profiles. Compared with the traditional PI control, the proposed MPPC method can stabilize better the dc voltage and is more robust to the consumption variation. Because the PI control method does not have the capability of grid voltage support by setting the active power reference, it has to maintain the dc-bus voltage by the dc-ac converter during the grid-connected operation mode, resulting inferior performance under the same condition of constant active power. In contrast to the traditional method, the proposed MPPC method can well maintain the stable dc-bus voltage by controlling the dc-dc converter, and the dc-ac converter can then be controlled to regulate the powers.

B. Fluctuant PV power generation

The proposed MPPC scheme is further tested and verified under the real-world fluctuating profiles of solar irradiation and ambient temperature, imitating the most severe situation of the PV output during a day as shown in Fig.12(a). The active and reactive power references are set as P_{ref} = -0.5MW and Q_{ref} = 0MVar. Load 3 (0.5MW ac load) is connected to the PCC initially. Load 1 (0.5MW dc load) is switched on at 1s. Load 2 (1MW dc load) is firstly switched on at 3s, and then switched off at 5s. At 5s, Load 4 (1MW ac load) is also connected, and then switched off at 7s.

As shown in Fig.12, the actual active and reactive powers at the PCC are maintained closely to their respective references. In the initial 3 seconds and the last 3 seconds, the ESS mainly absorbs the fluctuating PV power to keep the net power output from the dc-bus to the PCC continuously at around 0.5MW, and maintain stable and smooth dc-bus voltage. From 3s to 5s, the dc load capacity is greater than the PV output power, in order to maintain the stable dc-bus voltage stable, the ESS has to be discharged, as can be seen in the same period in Fig.12(e). Though there is a voltage swell on the dc-bus around 3.8s, the dc-bus regains its stability. From 5s to 7s, since an ac load is connected, the current passing through the PCC from the utility grid shows a steep rise in amplitude while the PCC power tracks P_{ref}, which demonstrates the effectiveness and robustness of the proposed MPPC scheme.

C. Flexible power regulation

Fig.13 shows dynamic tracking capability of the proposed MPPC scheme on the power references, where the solar irradiation and temperature are kept constant at 600W/m^2 and 25 ℃, respectively, yielding about 1.5MW power output. Load 3 (0.5MW ac load) is connected to the ac-bus initially. From 0s to 5s, Q_{ref} is set as 0Mvar, and P_{ref} as 0.2MW during 0s to 1s. Then, P_{ref} varies in the sequence of 0.7MW at 1s, -0.4MW at 2s, -0.7MW at 3s, 0.8MW at 4s, and it maintains 0.8MW afterwards. From 5s to 10s, Q_{ref} changes in the sequence of -0.02Mvar at 5s, 0.1Mvar at 6s, 0.04Mvar at 7s, -0.01Mvar at 8s, and 0.3Mvar at 9s and afterwards.

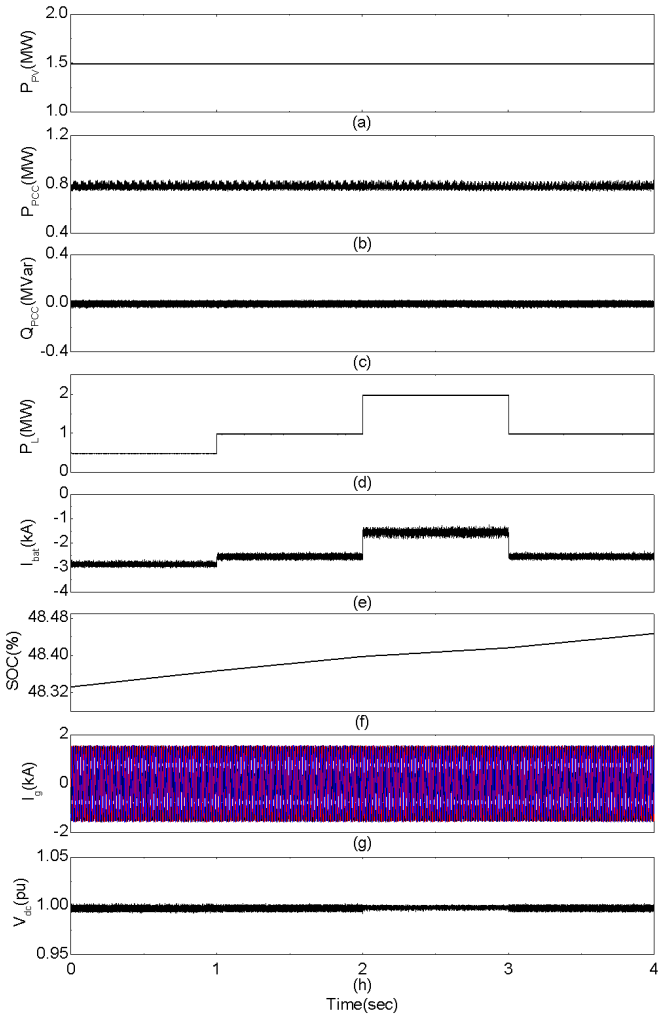

Fig.10. The performance of MPPC for dc-dc bidirectional converter under variable load demand condition: (a) PV power, (b) active power at PCC, (c) reactive power at PCC, (d) load power, (e) battery current, (f) SOC, (g) the current flowing between utility grid and PV-ESS system, (h) dc-bus voltage.

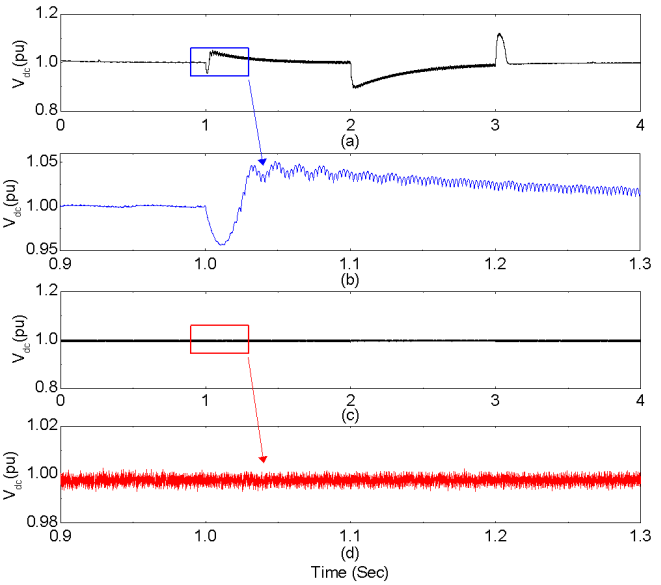

Fig.11. Comparison of the dc-bus voltages. (a)&(b) traditional method, (c)&(d) proposed method.

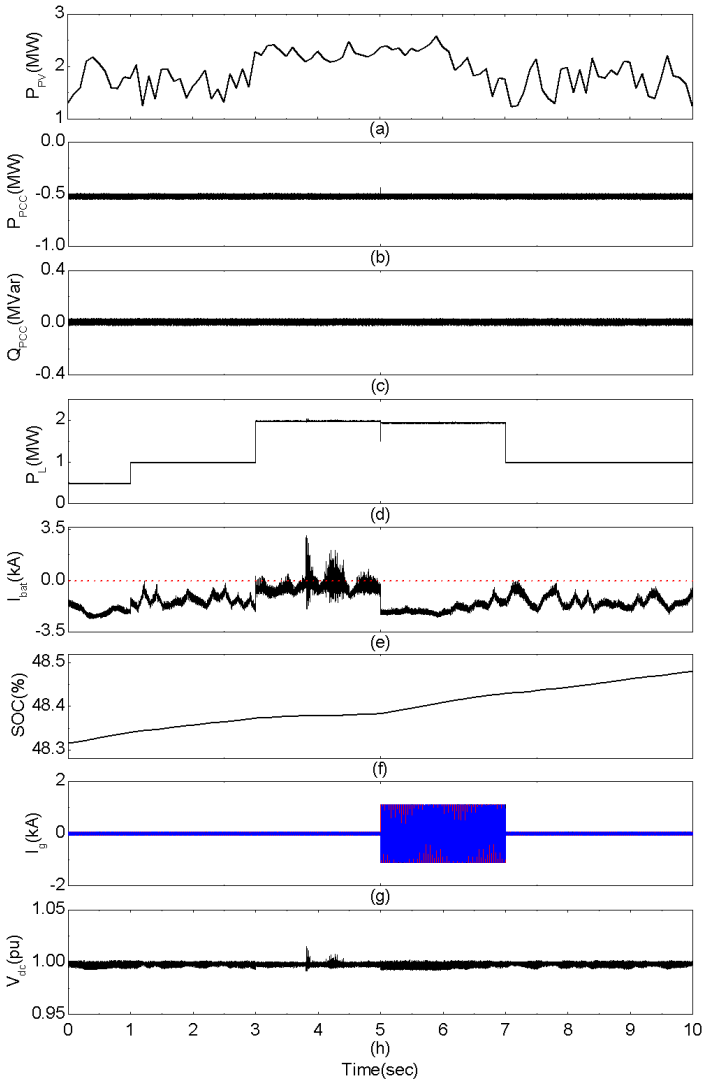

Fig.12. The performance under real-world fluctuant PV output using proposed method: (a) PV power, (b) active power at PCC, (c) reactive power at PCC, (d) load power, (e) battery current, (f) SOC, (g) the current flowing between utility grid and PV-ESS system, (h) dc-bus voltage.

For this PV-ESS system, it is reasonable that the references of power flows from grid to dc-bus (positive P_{ref} and positive Q_{ref}) are specified greater than those of the inverse power flows (negative P_{ref} and negative Q_{ref}) since the maximum load capacity is greater than that of the PV-ESS system. As shown in Fig.13, the active and reactive powers at PCC can track the references quickly and accurately.

D. Voltage support

In light of the aforementioned feature of flexible power regulation, the voltage support can be implemented. Since the active power regulation has a larger range than that of the reactive power, the voltage support can firstly employ the active power regulation. Fig.14 illustrates the voltage support performance through the active and reactive power flow regulation, respectively. Load 3 (0.5MW ac load) is connected initially. At 1s, Load 4 (1MW ac load) is switched on, leading to PCC voltage drop, which can be explained in Section III. Then, the voltage support strategy is activated at 1.5s by using (21) and (22), respectively. It can be observed that the voltage has been boosted up by about 2.20×10^{-3} pu as shown in Fig.14 (a) and 0.30×10^{-3} pu as shown in Fig.14 (b). Since the reactive power capacity is smaller than that of the active power, the voltage profile cannot be improved significantly by regulating the reactive power. With the high penetration of microgrids in the future grid, by coordinating the reactive power regulation of multiple microgrids, effective voltage support can be achieved.

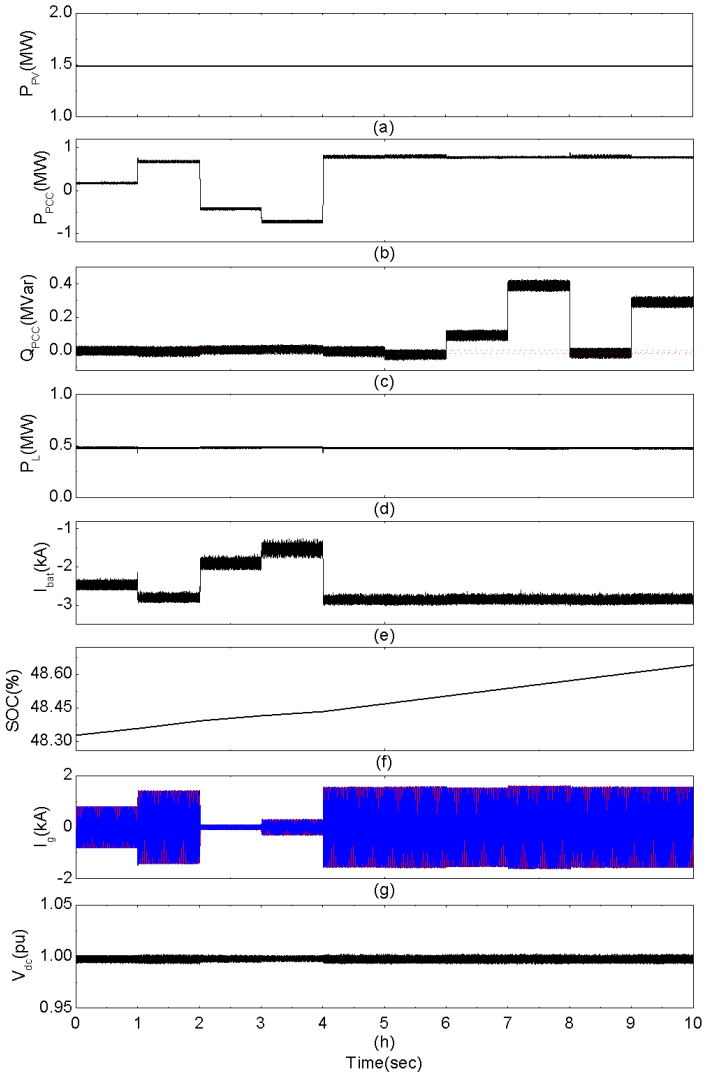

Fig.13. The performance of flexible power regulation using proposed method: (a) PV power, (b) active power at PCC, (c) reactive power at PCC, (d) load power, (e) battery current, (f) SOC, (g) the current flowing between utility grid and PV-ESS system, (h) dc-bus voltage.

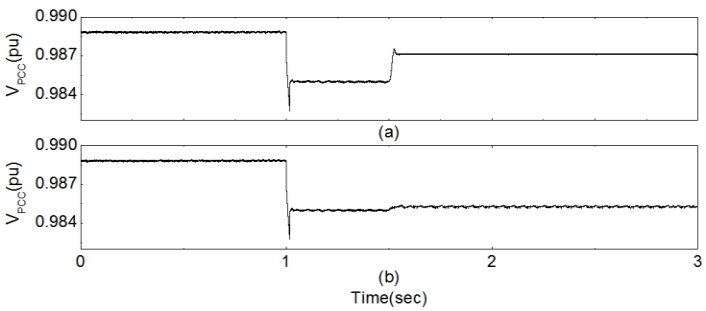

Fig.14. Voltage support performance of proposed method. (a) using active power flow control. (b) using reactive power flow control.

E. Robustness and stability

Using the evaluation and analysis method aforementioned in the Introduction [28], the robustness and stability of the proposed MPPC scheme to model parameter variations is evaluated here. Since the MPC control principle is based on the filter behaviors, so the parameters of both dc-side and ac-side filters are tested. On the dc side, dc-bus capacitor C_2 and battery associated inductor L_B are considered, while on the ac side, the filter's inductance L_f and resistance R_f are involved, which are all the key factors influencing the systemic dynamics. In these tests, the parameters are changed gradually in the controller while the parameters in the physical circuits in simulaiton are kept fixed according to Table I.

In the first test, C_2 is changed from 40mF to 60mF at a step of 1mF, while L_B from 0.1mH to 0.3mH at a step of 0.01mH. Load#1 is switched on, and the ac-side filter parameters are set according to Table I. For each combination of C_2 and L_B, one simulation model is created and run, resulting in 441 simulations, as shown in Fig. 15(a)&(b), where the dc-bus voltage ripple and the absolute error between the mean value and the rated value of the dc-bus voltage are plotted. Then, in the second test, L_f is changed from 0.1mH to 1.1mH at an interval of 0.05mH, and R_f is increased from 1mΩ to 3mΩ at an interval of 0.1mΩ. P_{ref} is set to 0.8MW. Q_{ref} is set to 0MVar. The inverter is supplied by a constant 1kV dc source. Once again, for each combination of L_f and R_f, one simulation model is created and run, resulting in another 441 simulations, as shown in Fig. 15(c), where the total harmonic distortion (THD) of the ac filter current are captured. Based on these two robustness tests, following features can be observed and discussed.

1) The proposed MPPC scheme is highly stable and robust against key control parameter variations. It can be seen that even under large mismatches, the system can also keep acceptable performance. For example, the maximum mismatch of dc side is the inductance, which is up to (0.30-0.17)/0.17=76.47%. Even so, the worst scenario only brings 6.86V dc-bus voltage ripple and 2.90V deviation from the rated value, as shown in Fig. 15(a) and (b), respectively.

2) From Fig.15(c), it can be seen that the choosing the same ac-side filter parameters in the controller as the actual physical ones leads to a low output current THD of 2.17%, and it is very close to the optimal value at 2.14%.

3) The controller can even perform better when the parameters in the controller are set to other values rather than the physical values. Taking Fig. 15(a) for example, if C_2 and L_B are set to 50mF and 0.17mH in the controller, respectively, which match the actual values in Table I, the resulting dc-bus voltage shows 0.824V deviation. However, if C_2 and L_B are set to around 59mF and 0.23mH respectively, the dc-bus voltage presents only 0.006V deviation.

4) Robustness and stability can be observed over a wide range of parameter variations around the nominal point. Therefore, accurate parameter setting is not of crucial significance for the proposed MPPC strategy.

F. Longer-horizon prediction

The impact of longer-horizon prediction on the performance of the proposed controller is analysed here. In the field of power converters, since the vast majority of discrete predictive models are developed by using Euler approximation, thus the control horizon is limited to one step and the focus of longer-horizon prediction lies in extending the prediction horizon.

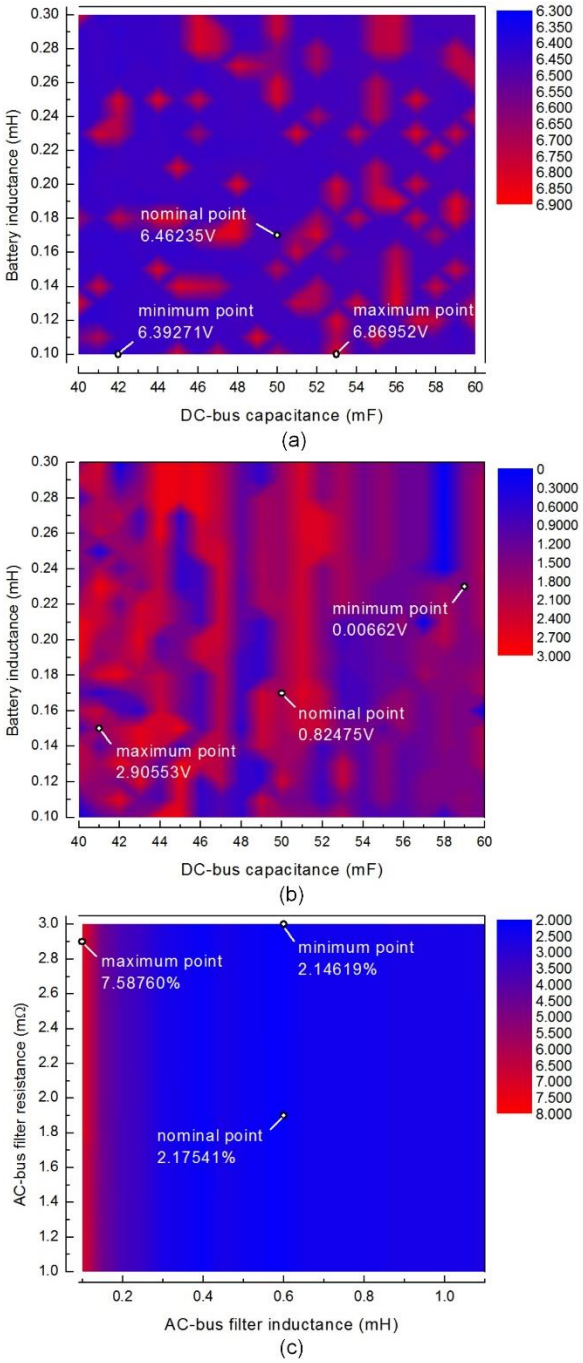

Fig.15. System performance under parameter variations: (a) dc-bus voltage ripple (V), (b) absolute error between mean value and rated value of the dc-bus voltage (V), (c) THD of ac filter current (%). Notice: nominal point means the result when the parameters in the controllers match those in the physical circuit.

All the predictive models, i.e. (2)-(3) and (15)-(16), at (k+1)th step can be rewritten as

$$\mathbf{x}(k+1) = A\mathbf{x}(k) + B\mathbf{u}(k) \tag{26}$$

where $\mathbf{x}$, $\mathbf{u}$ are system state variables, A, B are the coefficient matrices.

One more step prediction of (26) yields[34]

$$\mathbf{x}(k+2) = A\mathbf{x}(k+1) + B\mathbf{u}(k+1) \tag{27}$$

When prediction horizon N is more than 2, the linear extrapolation method is adopted [35]

$$\mathbf{x}(k+N) = \mathbf{x}(k+1) + (N-1)[\mathbf{x}(k+2) - \mathbf{x}(k+1)] \tag{28}$$

For consistency, both the dc-side and ac-side are with the same prediction horizon. Then longer-horizon prediction tests under proposed MPPC scheme are carried out, and the results are plotted in Fig.16 with the same evaluation criteria in the last subsection. As shown in Fig.16, curve 1 shows the dc-bus voltage ripple, curve 2 represents the absolute error of dc-bus mean voltage to the rated, and curve 3 indicates the THD of ac filter current. It can be seen that there are no significant variations for curves 1 and 2, whereas curve 3 presents a considerable increase when prediction horizon extends. This means a longer-horizon prediction would not necessarily bring a better performance due to the fact that the prediction accuracy could be compromised with a longer horizon. Based on this result, it is evident that N=1 is effective to control dc-bus voltage ripples and to limit the ac filter current THD. Therefore, one-step horizon prediction is simply adopted in this PV-Energy storage energy system.

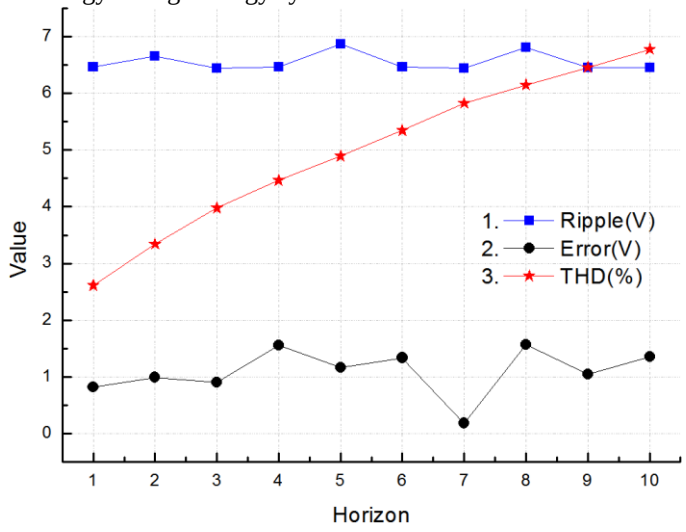

Fig.16. The effect of longer-horizon prediction on the performance of the system.

G. Comparison with existing MPC methods

In this subsection, the proposed MPPC scheme is compared with existing MPC methods. Traditionally, under grid-tied operation, the dc-bus voltage is supported by a rectifier (also called AFE) using MPC method with the active power reference obtained from an external PI controller whose inputs are the dc-bus voltage errors [14]. Simultaneously, dc-side dc-dc converter can be regulated by the MPC method with currents as the control objective in the cost function. The control diagram is depicted in Fig.17. The PI control parameters are given in the Table I, which are carefully tuned considering the trade off between dynamic response and steady-state errors.

For the sake of fairness, the variable load demand is the same as IV-A and the comparison is under the same battery current (mean value) which means I_B^* will be changed following the variable load demand. Q_{ref} is set to 0MVar. The results are shown in Fig.18. After analysis, the following observations can be made.

1) The dc-bus voltage by using the existing MPC method presents more oscillations than that by using the proposed MPPC scheme, especially when load varies at 2s, as shown in Fig. 18(a)&(b).

2) From Fig.18(b), the battery current ripple of the existing MPC method is less than that of the proposed scheme. This is because the current is formulated in the cost function and directly controlled by using the existing MPC. On the other hand, dc-bus voltage is the control objective of the proposed MPPC scheme. By doing so, the inverter is endowed with both flexible active and reactive power regulation capability.

3) At the ac side, the THD of the inverter output current by using the proposed MPPC scheme is 2.26%, lower than 2.81% of the existing MPC method. Due to the space limitation, the current waveforms are not plotted here.

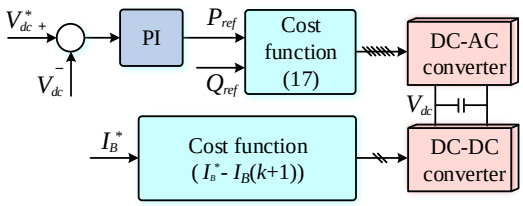

Fig.17. Existing MPC methods and their combination for the comparison.

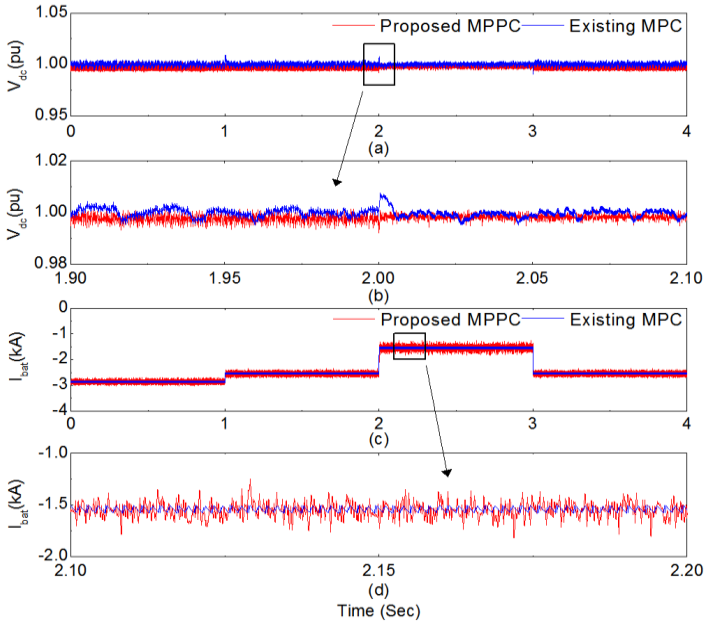

Fig.18. Comparison between existing MPC method and the proposed MPPC scheme: (a)&(b) dc-bus voltage, (c)&(d) battery current.

V. HARDWARE-IN-THE-LOOP TEST

The proposed control scheme is further validated in the controller hardware-in-the-loop (CHIL) test[36]. Fig.19 shows the experimental setup. In this CHIL, the proposed MPPC scheme is implemented in a DSP (TMS320F28335) controller, and other system components, such as the PV panels, ESS, and power converters are emulated by the OPAL-RT real-time simulator (RT-LAB OP4510). The system variables such as voltage and current are obtained from RT-LAB OP4510 and sent to the DSP to determine the optimal voltage vectors based on the MPPC algorithm. After that, the corresponding gate driving signals generated from the DSP is delivered back to RT-LAB OP4510 to control the dc-dc converter and the dc-ac inverter. In this test, initially, P_{ref} is set to 0.2MW and Q_{ref} as 0MVar. The solar irradiation and temperature are kept constant at 600W/m^2 and 25℃, respectively. Load 3 (0.5MW ac load) is connected to the ac-bus.

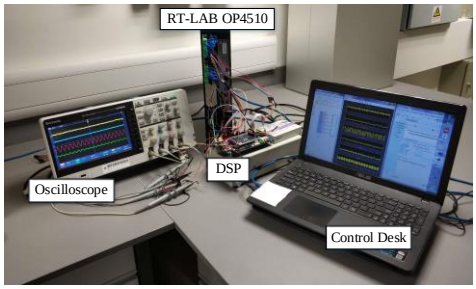

(a)

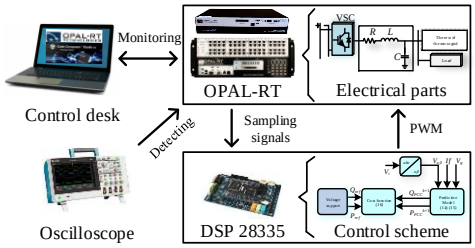

(b)

Fig.19. CHIL system. (a) laboratory setup. (b) schematic diagram.

Fig.20 presents the control signals produced by the DSP controller. The upper two are gate driving signals for the bidirecitional dc-dc converter for charging or discharging. The bottom two are the gate driving signals for one leg of the dc-ac converter. These signals are complementary and deadtime bands have been set. Note that the gate driving signals for the other two legs of the dc-ac converter are not shown here.

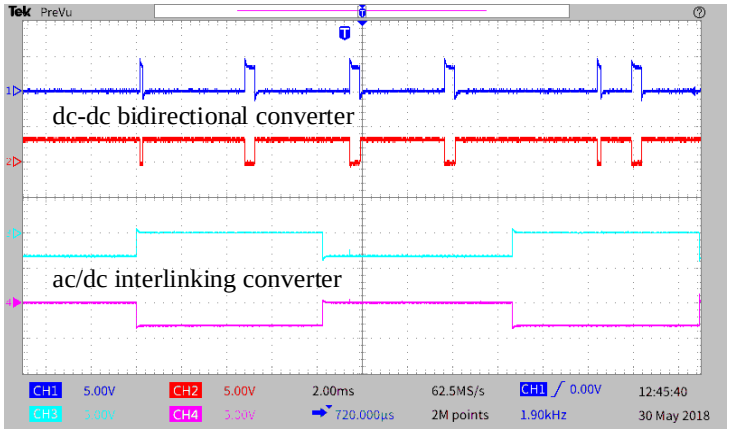

Fig.20. Gate drive signals.

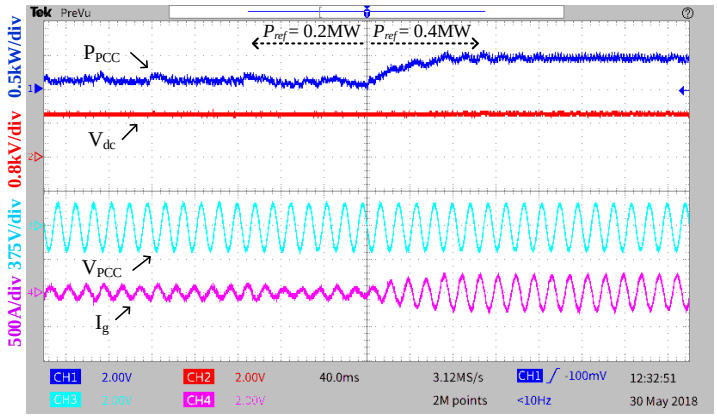

(a)

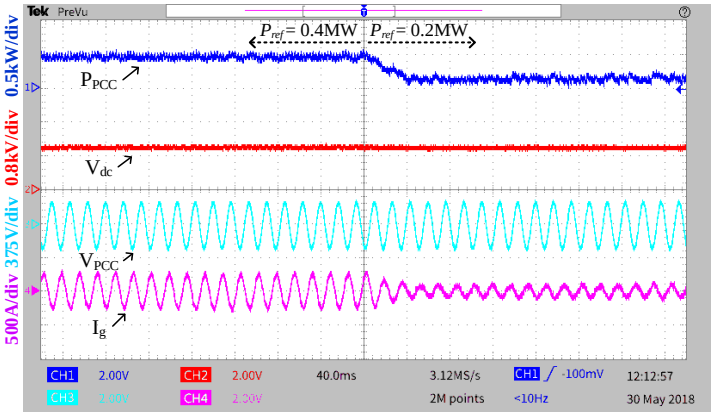

(b)

Fig.21. CHIL results when power reference changes. (a) active power reference steps up. (b) active power reference steps down.

Figs.21(a) and (b) show the results when P_{ref} steps up from 0.2MW to 0.4MW and steps down from 0.4MW to 0.2MW, respectively. As shown, the system can track the power reference dynamically within around 40ms to reach the new balance when the power reference varies. During this process, the dc-bus voltage is kept stable. As also shown in Fig.21 through the phase *a* voltage and current at the PCC, the system can provide a stable ac voltage supply. This verifies the effectiveness of proposed MPPC scheme in flexible power regulation and maintaining stable dc and ac voltages.

VI. Conclusion

This paper proposes an MPC-based MPPC scheme for a microgrid with PV-ESS systems. The MPPC for the dc-dc bidirectional converter aims to provide a stable and robust dc-bus voltage so as to smooth the influence from the fluctuating PV output, which otherwise will affect the grid voltage when the dc-bus is connected to the utility grid. Flexible power distribution can be achieved by providing stable dc- and ac-bus voltages, even under false power tracking. For the voltage dips caused by variable loads, a voltage support method is developed to compensate and restore the voltage drop. The proposed MPPC scheme is confirmed by numerical simulation and CHIL experimental test results for different scenarios.

References

[1] https://www.iea.org

[2] J. M. Guerrero, J. C. Vasquez, J. Matas, L. G. de Vicuna, and M. Castilla, "Hierarchical control of droop-controlled ac and dc microgrids – a general approach toward standardization", *IEEE Trans. Ind. Electron.*, vol. 58, no. 1, pp.158- 172, Jan. 2011.

[3] J. M. Carrasco, L.G. Franquelo, J.T. Bialasiewicz, E. Galvan, R.C. PortilloGuisado, M.A.M. Prats, J.I. Leon, and N. Moreno-Alfonso, "Power-electronic systems for the grid integration of renewable energy sources: a survey", *IEEE Trans. Ind. Electron.*, vol. 53, no. 4, pp.1002- 1016, Aug. 2006.

[4] D. E. Olivares, A. Mehrizi-Sani, A. H. Etemadi, C. A. Canizares, R. Iravani, M. Kazerani, A. H. Hajimiragha, O. Gomis-Bellmunt, M. Saeedifard, R. Palma-Behnke, G. A. Jimenez-Estevez, and N. D. Hatziargyriou, "Trends in microgrid control", *IEEE Trans. Smart Grid*, vol. 5, no. 4, pp.1905-1919, Jul. 2014.

[5] K. H. Ang, G. Chong and Y. Li, "PID control system analysis, design, and technology," *IEEE Trans. Control Syst. Technol.*, vol. 13, no. 5, pp. 1813–1827, Sep. 2014.

[6] M. Kwon and S. Choi, "Control Scheme for Autonomous and Smooth Mode Switching of Bidirectional DC–DC Converters in a DC Microgrid," *IEEE Trans. on Power Electron.*, vol. 33, no. 8, pp. 7094-7104, Aug. 2018.

[7] A. Pirooz and R. Noroozian, "Model predictive control of classic bidirectional DC-DC converter for battery applications," *2016 7th Power Electronics and*

Drive Systems Technologies Conference (PEDSTC), Tehran, 2016, pp. 517-522.

[8] Y. Mei, L. Chen, X. Li and K. Sun, "Model predictive control method for cascaded bi-directional DC-DC converter applied to a stand-alone photovoltaic energy storage system," *2016 19th International Conference on Electrical Machines and Systems (ICEMS)*, Chiba, 2016, pp. 1-5.

[9] A. Merabet, K. T. Ahmed, H. Ibrahim, R. Beguenane, and A. Ghias, "Energy management and control system for laboratory scale microgrid based wind-pv-battery," *IEEE Trans. Sustain. Energy*, vol. 8, no. 1, pp. 145–154, Jan. 2017.

[10] F. Nejabatkhah and Y. W. Li, "Overview of power management strategies of hybrid ac/dc microgrid", *IEEE Trans. Power Electron.*, vol. 30, no. 12, pp.7072- 7089, Dec. 2015.

[11] T. Ma, M. H. Cintuglu, and O. A. Mohammed, "Control of hybrid ac/dc microgrid involving energy storage and pulsed loads", *IEEE Trans. Ind. Appl*., vol. 53, no. 1, pp.567-575, Jan./Feb. 2017.

[12] A. Molina-Garcia, R. A. Mastromauro, T. Garcia-Sanchez, S. Pugliese, M. Liserre, and S. Stasi, "Reactive power flow control for pv inverters voltage support in LV distribution networks," *IEEE Trans. Smart Grid*, vol. 8, no. 1, pp. 447-456, Jan. 2017.

[13] J. Hu, Z. Li, J. Zhu and J. M. Guerrero, "Voltage stabilization: a critical step toward high photovoltaic penetration," *IEEE Ind. Electron. Mag*., vol. 13, no. 2, pp. 17-30, 2019.

[14] P. CortÉs, J. RodrÍguez, P. Antoniewicz and M. Kazmierkowski, "Direct Power Control of an AFE Using Predictive Control," *IEEE Trans. Power Electron.*, vol. 23, no. 5, pp. 2516-2523, Sep. 2008.

[15] D. E. Quevedo, R. P. Aguilera, M. A. Perez, P. Cortes and R. Lizana, "Model Predictive Control of an AFE Rectifier With Dynamic References," *IEEE Trans. Power Electron.*, vol. 27, no. 7, pp. 3128-3136, Jul. 2012.

[16] J. Hu, J. Zhu and D. G. Dorrell, "In-depth study of direct power control strategies for power converters," *IET Power Electron.*, vol. 7, no. 7, pp. 1810-1820, Jul. 2014.

[17] J. Hu and K. W. E. Cheng, "Predictive control of power electronics converters in renewable energy systems," *Energies*., vol. 10, no. 4, pp. 1-14, 2017.

[18] A. Parisio, E. Rikos, and L. Glielmo, "A model predictive control approach to microgrid operation optimization," *IEEE Trans. Control Syst. Technol*., vol. 22, no. 5, pp. 1813–1827, Sep. 2014.

[19] A. Ouammi, H. Dagdougui, L. Dessaint, and R. Sacile, "Coordinated model predictive-based power flows control in a cooperative network of smart microgrids," *IEEE Trans. Smart Grid*, vol. 6, no. 5, pp. 2233–2244, Sep. 2015.

[20] C. Sundstrom, D. Jung, and A. Blom, "Analysis of optimal energy management in smart homes using mpc", in Proc. of *European Control Conf.*, 2016, pp. 2066-2071.

[21] M. Moradzadeh, R. Boel and L. Vandevelde, "Voltage Coordination in Multi-Area Power Systems via Distributed Model Predictive Control," *IEEE Trans. on Power Syst.*, vol. 28, no. 1, pp. 513-521, Feb. 2013.

[22] M. Moradzadeh, R. Boel, and L. Vandevelde. "Anticipating and coordinating voltage control for interconnected power systems." *Energies*, vol. 7, no. 2, pp. 1027–1047, 2014.

[23] S. Vazquez, J. Rodriguez, M. Rivera, L. G. Franquelo and M. Norambuena, "Model Predictive Control for Power Converters and Drives: Advances and Trends," *IEEE Trans. Ind. Electron.*, vol. 64, no. 2, pp. 935-947, Feb. 2017.

[24] J. Hu, J. Zhu, G. Platt and D. G. Dorrell, "Model-predictive direct power control of ac/dc converters with one step delay compensation," in *Proc*. Of *Annual Conf.* on *IEEE Ind. Electron. Society*, 2012.

[25] J. Hu J. Zhu, and D. G. Dorrell, "Model predictive control of grid-connected inverters for PV systems with flexible power regulation and switching frequency reduction," *IEEE Trans. Ind. Appl*., vol. 51, no. 1, pp. 587-594, Jan./Feb. 2015.

[26] M. Lei, and et al, "An MPC-based ESS control method for PV power smoothing applications", *IEEE Trans. Power Electron.*, vol. 33, no. 3, pp. 2136– 2144, Mar. 2018.

[27] S. Kim, C. R. Park, J. Kim and Y. I. Lee, "A Stabilizing Model Predictive Controller for Voltage Regulation of a DC/DC Boost Converter," *IEEE Trans. Control Syst. Technol*., vol. 22, no. 5, pp. 2016-2023, Sep. 2014.

[28] T. Dragicevic, "Model predictive control of power converters for robust and fast operation of ac microgrids", *IEEE Trans. Power Electron*., vol. 33, no. 7, pp.6304-6317, Jul. 2018.

[29] Y. Shan, J. Hu, Z. Li and J. M. Guerrero, "A Model Predictive Control for Renewable Energy Based AC Microgrids Without Any PID Regulators," *IEEE Trans. Power Electron*., vol. 33, no. 11, pp. 9122-9126, Nov. 2018.

[30] A. N. Venkat, I. A. Hiskens, J. B. Rawlings and S. J. Wright, "Distributed MPC Strategies With Application to Power System Automatic Generation Control," *IEEE Trans. Control Syst. Technol*., vol. 16, no. 6, pp. 1192-1206, Nov. 2008.

[31] A. Olama, P. R. C. Mendes and E. F. Camacho, "Lyapunov-based hybrid model predictive control for energy management of microgrids," *IET Gener*., *Transmiss. Distrib.*, vol. 12, no. 21, pp. 5770-5780, Nov. 2018.

[32] Maryam Hashemi N. and V. Agelidis, "Evaluation of voltage regulation mitigation methods due to high penetration of PV generation in residential areas," *2013 International Conference on Renewable Energy Research and Applications (ICRERA)*, Madrid, 2013, pp. 1180-1189.

[33] M. Zeraati, M. E. H. Golshan, and J. M. Guerrero, "Distributed control of battery energy storage systems for voltage regulation in distribution networks with high pv penetration," *IEEE Trans. Smart Grid*, vol. 9, no. 4, pp. 3582-3593, Dec. 2018.

[34] P. Cortes, J. Rodriguez, C. Silva and A. Flores, "Delay Compensation in Model Predictive Current Control of a Three-Phase Inverter," *IEEE Trans. Ind. Electron.*, vol. 59, no. 2, pp. 1323-1325, Feb. 2012.

[35] J. Hu, J. Zhu and D. G. Dorrell, "Model predictive control of inverters for both islanded and grid-connected operations in renewable power generations," *IET Renewable Power Gener*., vol. 8, no. 3, pp. 240-248, Apr. 2014.

[36] J. Wang, C. Jin and P. Wang, "A Uniform Control Strategy for the Interlinking Converter in Hierarchical Controlled Hybrid AC/DC Microgrids," *IEEE Trans. Ind. Electron.*, vol. 65, no. 8, pp. 6188-6197, Aug. 2018.